Electron impact excitation of helium atom*

Han Xiao-Ying(韩小英)[a)†], Zeng De-Ling(曾德灵)[b)], Gao Xiang(高 翔)[c)], and Li Jia-Ming(李家明)[b)d)e)]

[a)] *Institute of Applied Physics and Computational Mathematics, Beijing* 100088, *China*
[b)] *Key Laboratory for Laser Plasmas (Ministry of Education) and Department of Physics and Astronomy, Shanghai Jiao Tong University, Shanghai* 200240, *China*
[c)] *Beijing Computational Science Research Center, Beijing* 100084, *China*
[d)] *Department of Physics and Center for Atomic and Molecular Nanosciences, Tsinghua University, Beijing* 100084, *China*
[e)] *Collaborative Innovation Center of Quantum Matter, Beijing* 100084, *China*

(Received 3 March 2015; revised manuscript received 13 April 2015; published online 20 June 2015)

A method to deal with the electron impact excitation cross sections of an atom from low to high incident energies are presented. This method combines the partial wave method and the first Born approximation (FBA), i.e., replacing the several lowest partial wave cross sections of the total cross sections within FBA by the corresponding exact partial wave cross sections. A new set of codes are developed to calculate the FBA partial wave cross sections. Using this method, the convergent e–He collision cross sections of optical-forbidden and optical-allowed transitions at low to high incident energies are obtained. The calculation results demonstrate the validity and efficiency of the method.

Keywords: electron impact excitation cross section, first Born approximation, partial wave method

PACS: 31.15.A–, 34.80.–i **DOI:** 10.1088/1674-1056/24/8/083103

1. Introduction

Atomic data of the electron impact excitation process are indispensable in many fields, including radiation physics,[1] plasma physics,[2] atmospheric physics,[3] and astrophysics.[3–5] Helium is an abundant element in the universe, whose electron impact excitation cross sections are important physical parameters for diagnosing helium abundances in astrophysics.[6–10]

With only two electrons, the helium atom provides a testing ground for developing a general method to deal with electron scattering with complex atoms or ions. Many calculations of electron–helium scattering have been performed experimentally (see review articles[11–14] and the references therein) and theoretically.[15–22] However, most of those studies mainly focused on the cross sections near the excitation threshold. Reference [21] (Fursa and Bray 1995) applied the convergent close-coupling (CCC) method to calculate e–He scattering cross section excited from the ground state in the incident energy range from 1.5 eV to 500 eV, where the overall agreement with the experimental data[23] is good, but without a detailed resonance structure.

It is known that the excitation cross sections of an atom impacted by low-energy electron can be dealt with by the partial wave method using *R*-matrix codes.[24–31] At the high incident energy, the first Born approximation (FBA) is applicable and the generalized oscillator strength (GOS, i.e. the differential cross sections) can be calculated, e.g., by the codes we developed from the traditional *R*-matrix codes.[32,33] To calculate the electron impact excitation cross sections of the atom at intermediate incident energy is still a difficult task, especially for optical-allowed transition, since here FBA is inapplicable and a huge number of partial wave cross sections (PWCS's) need to be accounted.

In this work, an approach to deal with the electron impact excitation cross sections of atom at low to high incident energies in a consistent way are presented and validated by the e–He collision calculations. More specifically, the exact PWCS's and the PWCS's within FBA of e–He collision in the whole energy range (from low to high incident energies) are calculated for $[1s^2]1^1S \rightarrow [1s2s]2^1S$ and $[1s^2]1^1S \rightarrow [1s2p]2^1P$ transitions. The exact PWCS's are calculated by using the traditional *R*-matrix method. To calculate the PWCS's within FBA, a new set of codes are developed based on the traditional *R*-matrix codes. The calculation results show that the two kinds of PWCS's decrease with the increasing angular momentum L and the increasing incident energy. The comparisons between the two kinds of PWCS's manifest that the exact and FBA PWCS's merge together gradually with the increasing L. The two features give some hint that the difference between the exact and FBA total cross sections mainly originate from the lowest several PWCS's. Thus the approach of combining the partial wave method and FBA is presented, i.e., replacing a few FBA PWCS's ($L < L_{\rm cut}$) of the FBA total cross sections by the corresponding exact PWCS's. The

*Project supported by the National Basic Research Program of China (Grant Nos. 2011CB921501 and 2013CB922200), the National Natural Science Foundation of China (Grant Nos. 11274035, 11275029, 11328401, 11371218, 11474031, 11474032, and 11474034), and the Foundation of Development of Science and Technology of Chinese Academy of Engineering Physics (Grant Nos. 2013A0102005 and 2014A0102005).

†Corresponding author. E-mail: han_xiaoying@iapcm.ac.cn

© 2015 Chinese Physical Society and IOP Publishing Ltd

convergent total cross sections of e–He collision for monopole and dipole transitions at low to high incident energies are obtained by using this method. Our calculation results agree with the previous experimental measurement[23] and CCC calculation results[21] overall. Moreover, in our calculations the resonance structures near the excitation threshold are displayed. Therefore, the e–He collision calculations demonstrate that the excitation cross sections of an atom impacted by electrons at low to high incident energies can be dealt with efficiently in a consistent way by combining the partial wave method and FBA.

2. Theoretical method

2.1. *R*-matrix method

Since the detailed descriptions of the *R*-matrix method to deal with the electron–atom collision process have been presented elsewhere,[24–31] a brief outline will be given here. This method begins by partitioning the subconfiguration space of the colliding electron into two regions by a sphere of radius a centered on the nucleus. The value of a is chosen such that the exchange interactions between the colliding electron and the other target electrons are negligible for $r > a$, where r is the distance of the colliding electron relative to the centroid of the target atom. Thus in the external region ($r \geq a$), the colliding electron mainly feels a long-range static polarization potentials.

Within the reaction zone $r \leq a$, the interactions between the colliding electron and the target electrons involve electron exchange and correlation interactions, which is a many-body problem and is solved variationally as a whole to obtain the logarithmic derivative boundary matrix $R(E)$. Therefore, in the reaction-zone the electron correlations for the $(N+1)$-electron system including the target atom and a colliding electron are calculated adequately by the variational method. The wavefunction Ψ for the $(N+1)$-electron system of eigenenergy E in the reaction zone are expanded as

$$\Psi = \sum_k A_{E_k} \Psi_k, \tag{1}$$

where Ψ_k are the energy-independent bases, which are expanded by the following way

$$\Psi_k = A \sum_{ij} a_{ijk} \Phi_i \frac{1}{r_{N+1}} u_{ij}(r_{N+1}) + \sum_j b_{jk} \phi_j, \tag{2}$$

where A is the antisymmetrization operator which accounts for the electron exchange between the target electrons and the colliding electron. Φ_i are the channel wavefunctions obtained by coupling the N-electron target wave functions with the angular momentum and spin of the colliding electron. u_{ij} are the continuum orbitals. ϕ_j are $(N+1)$-electron wave functions formed from the bound-type orbitals to ensure the completeness of the total wave functions and take account of the electron correlations within the reaction zone. The coefficients a_{ijk} and b_{jk} are obtained by diagonalizing the Hamiltonian matrix of the $(N+1)$-electron system. Using the *R*-matrix method, we can deal with the interactions between the target electrons and the colliding electron in various channels within the reaction zone.

2.2. Scattering amplitude

In an electron impact excitation process, the differential cross section $\mathrm{d}\sigma/\mathrm{d}\Omega$ is equal to $(k'/k)|f(\hat{k}')|^2$ (atomic units are used throughout the paper if not specified). Here $f(\hat{k}')$ is the scattering amplitude, which can be calculated by the following formula,[34]

$$\begin{aligned} f_{i\to j}(\hat{k}') &= -\frac{1}{2\pi} T_{i\to j} = -\frac{1}{2\pi} \langle \mathrm{e}^{\mathrm{i}\boldsymbol{k}'\cdot\boldsymbol{r}} \chi', \Phi_j(\tilde{L}'\tilde{S}'\tilde{\pi}') | V(\boldsymbol{r}_1 \cdots \boldsymbol{r}_N, \boldsymbol{r}) | \Psi^+ \rangle \\ &= -\frac{1}{2\pi} \langle \mathrm{e}^{\mathrm{i}\boldsymbol{k}'\cdot\boldsymbol{r}} \chi', \Phi_j(\tilde{L}'\tilde{S}'\tilde{\pi}') | T | \mathrm{e}^{\mathrm{i}\boldsymbol{k}\cdot\boldsymbol{r}} \chi, \Phi_i(\tilde{L}\tilde{S}\tilde{\pi}) \rangle = \sum_{LS\pi} f_{i\to j}^{LS\pi}(\hat{k}'), \end{aligned} \tag{3}$$

where $T_{i\to j}$ is the T-matrix. $\boldsymbol{k}$ ($\boldsymbol{k}'$) and χ (χ') are the wave vector and spin wave function of the initial (final) state of the impact electron. $\Phi_i(\tilde{L}\tilde{S}\tilde{\pi})$ and $\Phi_j(\tilde{L}'\tilde{S}'\tilde{\pi}')$ are the initial- and final-state wave functions of the target with the definite angular momentum $\tilde{L}$ ($\tilde{L}'$), spin $\tilde{S}$ ($\tilde{S}'$), and parity $\tilde{\pi}$ ($\tilde{\pi}'$). $|\mathrm{e}^{\mathrm{i}\boldsymbol{k}\cdot\boldsymbol{r}}\chi, \Phi(\tilde{L}\tilde{S}\tilde{\pi})\rangle$ is the wave function of an $(N+1)$-electron system. Ψ^+ characterizes the asymptotic behavior of the initial state for the $(N+1)$-electron system. $V(\boldsymbol{r}_1 \cdots \boldsymbol{r}_N, \boldsymbol{r})$ is the interaction operator between the impact electron and the target, which is equal to $\sum_{\alpha=1}^{N} \frac{-1}{|\boldsymbol{r}-\boldsymbol{r}_\alpha|} + Z/\boldsymbol{r}$ (Z is the charge of the atomic nucleus) if the interaction is Coulombic. N is the number of electrons in the target. $\boldsymbol{r}$ and $\boldsymbol{r}_\alpha$ are, respectively, the coordinates of the impact electron and the α-th electron in the target relative to the centroid of the target. The partial wave scattering amplitude $f_{i\to j}^{LS\pi}(\hat{k}')$ is

$$f_{i\to j}^{LS\pi}(\hat{k}') = -\mathrm{i}\sqrt{\frac{\pi}{kk'}} \sum_{ll'} \sum_{m_s} \sum_{m_{l'} m_{s'}} \mathrm{i}^{l-l'} (2l+1)^{1/2} \mathrm{Y}_{l'm_{l'}}(\hat{k}') T_{i\to j}^{LS\pi} \langle \tilde{L}'\tilde{M}'_{\tilde{L}'}, l'm_{l'} | LM_L \rangle$$

$$\cdot \langle \tilde{S}' \tilde{M}'_{\tilde{S}'}, s' m_{s'} | S M_S \rangle \langle L M_L | \tilde{L} \tilde{M}_{\tilde{L}}, l0 \rangle \langle S M_S | \tilde{S} \tilde{M}_{\tilde{S}}, s m_s \rangle, \tag{4}$$

here the direction of incident electron is defined as the $\hat{z}$ axis. l (l') and s (s') are the angular momentum and spin of the impact (scattered) electron. The total angular momentum L, spin S, and parity π of the $(N+1)$-electron system are good quantum numbers in an electron impact process. $T_{i\to j}^{LS\pi}$ are the reduced transition matrix elements in $LS\pi$ representation, which only connect the initial and final states with the same $LS\pi$ because of the conservation of the good quantum numbers. Moreover, $T_{i\to j}^{LS\pi}$ are independent of the magnetic quantum numbers because of the rotational invariance of the scattering interaction. In this work, we adopt the set $2'$ orbital basis of Ref. [20] to calculate the e–He collision excitation cross sections by the partial wave method using the FARM code.[35] More specifically, the adopted orbital basis includes the spectroscopy orbitals nl ($n = 1$–3, $l = 0$–2) and the pseudo orbitals $\bar{n}l$ ($\bar{n} = 4$–6, $l = 0$–4), and 11 physical states are used to expand the $(N+1)$-electron system. The detailed description of the procedure to prepare the orbital basis and the convergence of the calculated total cross sections based on the basis can be found in Ref. [20]. In this work we only extend the calculations to a higher incident energy range.

2.3. Generalized oscillator strength

According to Bethe theory,[36,37] if the incident energy of the impact electron is high enough, the asymptotic wave function Ψ^+ of the $(N+1)$-electron system can be evaluated by $|\mathrm{e}^{\mathrm{i}\boldsymbol{k}\cdot\boldsymbol{r}}\chi, \Phi_i(\tilde{L}\tilde{S}\tilde{\pi})\rangle$ within FBA,[38] and the corresponding FBA amplitude is

$$\begin{aligned} f_{i\to j}^{(\mathrm{FBA})}(\hat{k}') &= -\frac{1}{2\pi} T_{i\to j}^{(\mathrm{FBA})} = -\frac{1}{2\pi} \langle \mathrm{e}^{\mathrm{i}\boldsymbol{k}'\cdot\boldsymbol{r}}\chi', \Phi_j(\tilde{L}'\tilde{S}'\tilde{\pi}') | V | \mathrm{e}^{\mathrm{i}\boldsymbol{k}\cdot\boldsymbol{r}}\chi, \Phi_i(\tilde{L}\tilde{S}\tilde{\pi}) \rangle \\ &= -\frac{2}{K^2} \langle \Phi_j(\tilde{L}'\tilde{S}'\tilde{\pi}') | \sum_{\alpha=1}^{N} \mathrm{e}^{\mathrm{i}\boldsymbol{K}\cdot\boldsymbol{r}_\alpha} | \Phi_i(\tilde{L}\tilde{S}\tilde{\pi}) \rangle, \end{aligned} \tag{5}$$

where $T_{i\to j}^{(\mathrm{FBA})}$ is the T-matrix within FBA. $\boldsymbol{K} = \boldsymbol{k} - \boldsymbol{k}'$ is the momentum transfer of the impact electron. In the last line of Eq. (5), the coordinate $\boldsymbol{r}$ of the impact electron is integrated[38] and the infinite partial wave cross sections are calculated as a whole.

The generalized oscillator strength (GOS) $F_{i\to j}(\Delta E, K)$ of the target is defined as,

$$\begin{aligned} & F_{i\to j}(\Delta E, K) \\ &= \frac{2\Delta E}{K^2} \left| \langle \Phi_j(\tilde{L}'\tilde{S}'\tilde{\pi}') | \sum_{\alpha=1}^{N} \mathrm{e}^{\mathrm{i}\boldsymbol{K}\cdot\boldsymbol{r}_\alpha} | \Phi_i(\tilde{L}\tilde{S}\tilde{\pi}) \rangle \right|^2 \\ &= \frac{K^2 \Delta E}{2} |f_{i\to j}^{(\mathrm{FBA})}(\hat{k}')|^2. \end{aligned} \tag{6}$$

From Eq. (6), we can see that the accuracy of GOS is determined by the accuracy of the target wave function $\Phi(\tilde{L}\tilde{S}\tilde{\pi})$. Moreover, in the limit of $K \to 0$, GOS is equal to the optical oscillator strength (OOS), which will be useful to test the accuracy of the calculated GOS by using the optical experimental measurement. In our previous work,[32] the high precision GOS of helium excited from the ground state to $n^1\mathrm{S}$, $n^1\mathrm{P}$, $n^1\mathrm{D}$ ($n \to \infty$) and adjacent continuum states are calculated by using our developed codes.

2.4. Total and partial wave cross sections within FBA

Within FBA, the relation between the differential cross section $\mathrm{d}\sigma_{i\to j}^{(\mathrm{FBA})}/\mathrm{d}\Omega$ and transition matrix $T_{i\to j}^{(\mathrm{FBA})}$ is

$$\frac{\mathrm{d}\sigma_{i\to j}^{(\mathrm{FBA})}}{\mathrm{d}\Omega} = \frac{1}{4\pi^2} \frac{k'}{k} |T_{i\to j}^{(\mathrm{FBA})}|^2. \tag{7}$$

After performing the summation of the final state and the average of the initial state, i.e. the integration of $\hat{k}'$, and the sum of $\tilde{M}'_{\tilde{L}'}$, $\tilde{M}'_{\tilde{S}'}$, and $m'_{s'}$, and the average over $\hat{k}$, $\tilde{M}_{\tilde{L}}$, $\tilde{M}_{\tilde{S}}$, and m_s, we obtain the FBA total cross sections $\sigma_{i\to j}^{(\mathrm{FBA})}$,

$$\begin{aligned} \sigma_{i\to j}^{(\mathrm{FBA})} &= \frac{1}{4\pi} \int \frac{\mathrm{d}\sigma_{i\to j}^{(\mathrm{FBA})}}{\mathrm{d}\Omega} \mathrm{d}\hat{k}\mathrm{d}\hat{k}' \\ &= \frac{1}{4\pi} \int \frac{1}{4\pi^2} \frac{k'}{k} \frac{1}{[\tilde{L}][\tilde{S}][s]} \\ &\quad \times \sum_{\tilde{M}_{\tilde{L}}\tilde{M}_{\tilde{S}} m_s} \sum_{\tilde{M}'_{\tilde{L}'}\tilde{M}'_{\tilde{S}'} m'_{s'}} |T_{i\to j}^{(\mathrm{FBA})}|^2 \mathrm{d}\hat{k}\mathrm{d}\hat{k}', \end{aligned} \tag{8}$$

where $[\tilde{L}]$ means $2\tilde{L}+1$ and $|T_{i\to j}^{(\mathrm{FBA})}|^2$ can be expanded as

$$\begin{aligned} |T_{i\to j}^{(\mathrm{FBA})}|^2 &= |\langle \mathrm{e}^{\mathrm{i}\boldsymbol{k}'\cdot\boldsymbol{r}}\chi', \Phi_j(\tilde{L}'\tilde{S}'\tilde{\pi}') | V | \mathrm{e}^{\mathrm{i}\boldsymbol{k}\cdot\boldsymbol{r}}\chi, \Phi_i(\tilde{L}\tilde{S}\tilde{\pi}) \rangle|^2 \\ &= \Bigg(\sum_{l m_l l' m'_{l'}} (4\pi)^2 i^{l-l'} \mathrm{Y}^*_{l m_l}(\hat{k}) \mathrm{Y}_{l' m'_{l'}}(\hat{k}') \\ &\quad \cdot \sum_{LSM_L M_S \pi} C^{LM_L}_{\tilde{L}'\tilde{M}'_{\tilde{L}'}, l' m'_{l'}} C^{SM_S}_{\tilde{S}'\tilde{M}'_{\tilde{S}'}, s' m'_{s'}} \\ &\quad \times C^{LM_L}_{\tilde{L}\tilde{M}_{\tilde{L}}, l m_l} C^{SM_S}_{\tilde{S}\tilde{M}_{\tilde{S}}, s m_s} T^{(FBA)LS\pi}_{i\to j} \Bigg) \\ &\quad \cdot \Bigg(\sum_{\bar{l}\bar{m}_{\bar{l}}\bar{l}'\bar{m}'_{\bar{l}'}} (4\pi)^2 (-\mathrm{i})^{\bar{l}-\bar{l}'} \mathrm{Y}_{\bar{l}\bar{m}_{\bar{l}}}(\hat{k}) Y^*_{\bar{l}'\bar{m}'_{\bar{l}'}}(\hat{k}') \\ &\quad \cdot \sum_{\bar{L}\bar{S}\bar{M}_{\bar{L}}\bar{M}_{\bar{S}}\pi} C^{\bar{L}\bar{M}_{\bar{L}}}_{\tilde{L}'\tilde{M}'_{\tilde{L}'}, \bar{l}'\bar{m}'_{\bar{l}'}} C^{\bar{S}\bar{M}_{\bar{S}}}_{\tilde{S}'\tilde{M}'_{\tilde{S}'}, s' m'_{s'}} \\ &\quad \times C^{\bar{L}\bar{M}_{\bar{L}}}_{\tilde{L}\tilde{M}_{\tilde{L}}, \bar{l}\bar{m}_{\bar{l}}} C^{\bar{S}\bar{M}_{\bar{S}}}_{\tilde{S}\tilde{M}_{\tilde{S}}, s m_s} T^{*(FBA)\bar{L}\bar{S}\pi}_{i\to j} \Bigg). \end{aligned} \tag{9}$$

According to the orthogonality of the Clebsch–Gordon coefficient and spherical harmonic functions, we obtain

$$\begin{aligned}
&\int \mathrm{Y}^*_{lm_l}(\hat{k})\mathrm{Y}_{\bar{l}\bar{m}_{\bar{l}}}(\hat{k})\,\mathrm{d}\hat{k} = \delta_{l\bar{l}}\delta_{m_l\bar{m}_{\bar{l}}},\\
&\int \mathrm{Y}^*_{l'm'_{l'}}(\hat{k}')\mathrm{Y}_{\bar{l}'\bar{m}'_{\bar{l}}}(\hat{k}')\,\mathrm{d}\hat{k}' = \delta_{l'\bar{l}'}\delta_{m_{l'}\bar{m}_{\bar{l}'}},\\
&\sum_{\tilde{M}'_{\tilde{S}'}m'_{s'}} C^{SM_S}_{\tilde{S}'\tilde{M}'_{\tilde{S}'},s'm'_{s'}} C^{\bar{S}\bar{M}_{\bar{S}}}_{\tilde{S}'\tilde{M}'_{\tilde{S}'},s'm'_{s'}} = \delta_{S\bar{S}}\delta_{M_S\bar{M}_{\bar{S}}},\\
&\sum_{\tilde{M}_{\tilde{S}}m_s} C^{SM_S}_{\tilde{S}\tilde{M}_{\tilde{S}},sm_s} C^{\bar{S}\bar{M}_{\bar{S}}}_{\tilde{S}\tilde{M}_{\tilde{S}},sm_s} = \delta_{S\bar{S}}\delta_{M_S\bar{M}_{\bar{S}}},\\
&\sum_{\tilde{M}'_{\tilde{L}'}m'_{l'}} C^{LM_L}_{\tilde{L}'\tilde{M}'_{\tilde{L}'},l'm'_{l'}} C^{\bar{L}\bar{M}_{\bar{L}}}_{\tilde{L}'\tilde{M}'_{\tilde{L}'},l'm'_{l'}} = \delta_{L\bar{L}}\delta_{M_L\bar{M}_{\bar{L}}},\\
&\sum_{\tilde{M}_{\tilde{L}}m_l} C^{LM_L}_{\tilde{L}\tilde{M}_{\tilde{L}},lm_l} C^{\bar{L}\bar{M}_{\bar{L}}}_{\tilde{L}\tilde{M}_{\tilde{L}},lm_l} = \delta_{L\bar{L}}\delta_{M_L\bar{M}_{\bar{L}}}. \qquad (10)
\end{aligned}$$

So the total cross section within FBA is

$$\begin{aligned}
\sigma^{(\mathrm{FBA})}_{i\to j} &= \frac{8\pi k'}{k}\frac{1}{[\tilde{L}][\tilde{S}]}\sum_{LS\pi ll'}[L][S]|T^{(FBA)LS\pi}_{i\to j}|^2\\
&= \frac{8\pi k'}{k}\frac{1}{[\tilde{L}][\tilde{S}]}\sum_{LS\pi ll'}[L][S]|\langle\gamma'\tilde{L}'\tilde{S}'l's';LS|\\
&\quad\times\sum_{\alpha=1}^{N}\frac{1}{|\boldsymbol{r}-\boldsymbol{r}_\alpha|}|\gamma\tilde{L}\tilde{S}ls;LS\rangle|^2 = \sum_{LS\pi}\sigma^{(FBA)LS\pi}_{i\to j}, \qquad (11)
\end{aligned}$$

where γ represents all the other information to define the target state uniquely. Based on the traditional R-matrix codes we develop a new set of codes to calculate the PWCS's within FBA presented in formula (11). In this work, we adopt the same set of orbital bases, including spectroscopy orbitals 1s, 2s, 2p, 3s, 3p, 3d and pseudo-orbitals $\bar{4}$s, $\bar{4}$p, $\bar{4}$d used in our previous helium GOS calculations,[32] to calculate the e–He collision excitation PWCS's within FBA by using our updated codes.

The difference between the exact PWCS and the FBA PWCS is

$$\sigma^{(\mathrm{C})}_L = \sigma^{(\mathrm{Exact})}_L - \sigma^{(\mathrm{FBA})}_L. \qquad (12)$$

If $\sigma^{(\mathrm{C})}_L$ decreases fast with the increasing angular momentum L, the convergent total cross sections can be obtained by the FBA total cross sections plus limited $\sigma^{(\mathrm{C})}_L$, i.e.

$$\begin{aligned}
\sigma^{(\mathrm{Exact})}_{\mathrm{total}} &= \sigma^{(\mathrm{FBA})}_{\mathrm{total}} + \sum_{L=0}^{L_{\mathrm{cut}}}\sigma^{(\mathrm{C})}_L\\
&= \sigma^{(\mathrm{FBA})}_{\mathrm{total}} + \sum_{L=0}^{L_{\mathrm{cut}}}\left(\sigma^{(\mathrm{Exact})}_L - \sigma^{(\mathrm{FBA})}_L\right). \qquad (13)
\end{aligned}$$

It means that a few lowest FBA PWCS's ($L \le L_{\mathrm{cut}}$) of the total cross sections within FBA are replaced by the corresponding exact PWCS's. Beyond L_{cut} the difference between the exact and FBA PWCS's is negligible. This approach is anticipated to be more efficient than the partial wave method to calculate the total cross sections at intermediate incident energy, especially for the optical-allowed transition.

3. Results and discussion

3.1. Monopole transition

Figure 1 shows the comparisons between our calculated eight lowest PWCS's ($L = 0 \sim 7$) for $[1s^2]1^1S \to [1s2s]2^1S$ transition according to the formula (4) (labeled as "Exact") and the formula (11) (labeled as "FBA") respectively. In Fig. 1, it can be seen that the two kinds of PWCS's decrease fast with the increasing angular momentum L and the increasing incident energy. The maximum of the two kinds of PWCS's for $L = 7$ are only about 10% of those for $L = 0$ respectively. The two kinds of PWCS curves gradually merge together with the increasing L at the intermediate and high incident energies (> 200 eV). So the main contribution of the differences between $\sigma^{(\mathrm{Exact})}_{\mathrm{total}}$ and $\sigma^{(\mathrm{FBA})}_{\mathrm{total}}$ should originate from the several lowest PWCS's. In addition, it can be seen that the resonance structures mainly present in the low exact PWCS's with $L \le 5$ near the excitation threshold. No resonance structure appears in the FBA PWCS's.

Figure 2 shows the total cross sections for $[1s^2]1^1S \to [1s2s]2^1S$ transition calculated by partial wave method and FBA method respectively. In Fig. 2, at the low incident energies (from threshold to 50 eV) the blue, red, and black dashed lines (corresponding to the summations of the lowest 6, 11, and 16 $\sigma^{(\mathrm{Exact})}_L$ respectively) nearly merge together; while at the higher incident energies, their difference becomes larger. It seems that the summations of 11 and 16 $\sigma^{(\mathrm{Exact})}_L$ agree to the CCC results in the overall energy range while the summation of 6 $\sigma^{(\mathrm{Exact})}_L$ is smaller at incident energies larger than 50 eV. This manifests that a convergence of the total cross sections near threshold ($E_i < 50$ eV) can be obtained by counting the lowest 6 PWCS's for the optical-forbidden transition, while at intermediate and high incident energies ($E_i > 50$ eV) 11 or even 16 PWCS's are necessary to be accounted. On the other hand, within FBA the summation of the lowest 11 $\sigma^{(\mathrm{FBA})}_L$ is close to $\sigma^{(\mathrm{FBA})}_{\mathrm{total}}$ while the summation of the lowest 6 $\sigma^{(\mathrm{FBA})}_L$ is lower than $\sigma^{(\mathrm{FBA})}_{\mathrm{total}}$. At high incident energies ($E_i > 400$ eV), the summation of 11 $\sigma^{(\mathrm{Exact})}_L$ and the summation of 11 $\sigma^{(\mathrm{FBA})}_L$ merge together, which means the FBA is applicable here.

$\sigma^{(\mathrm{C})}_L$ is the difference between $\sigma^{(\mathrm{Exact})}_L$ and $\sigma^{(\mathrm{FBA})}_L$. In Fig. 2, the solid curves, corresponding to $\sigma^{(\mathrm{FBA})}_{\mathrm{total}} + \sum_{L=0-5}\sigma^{(\mathrm{C})}_L$ (blue) and $\sigma^{(\mathrm{FBA})}_{\mathrm{total}} + \sum_{L=0-10}\sigma^{(\mathrm{C})}_L$ (red) respectively, agree with our convergent results (the red and black dashed curves calculated by partial wave method). This means the approach to calculate the total cross sections at low to high incident energies, i.e., replacing a few FBA PWCS's ($L < L_{\mathrm{cut}}$) of the FBA total cross sections by the corresponding exact PWCS's, is applicable for the monopole transition.

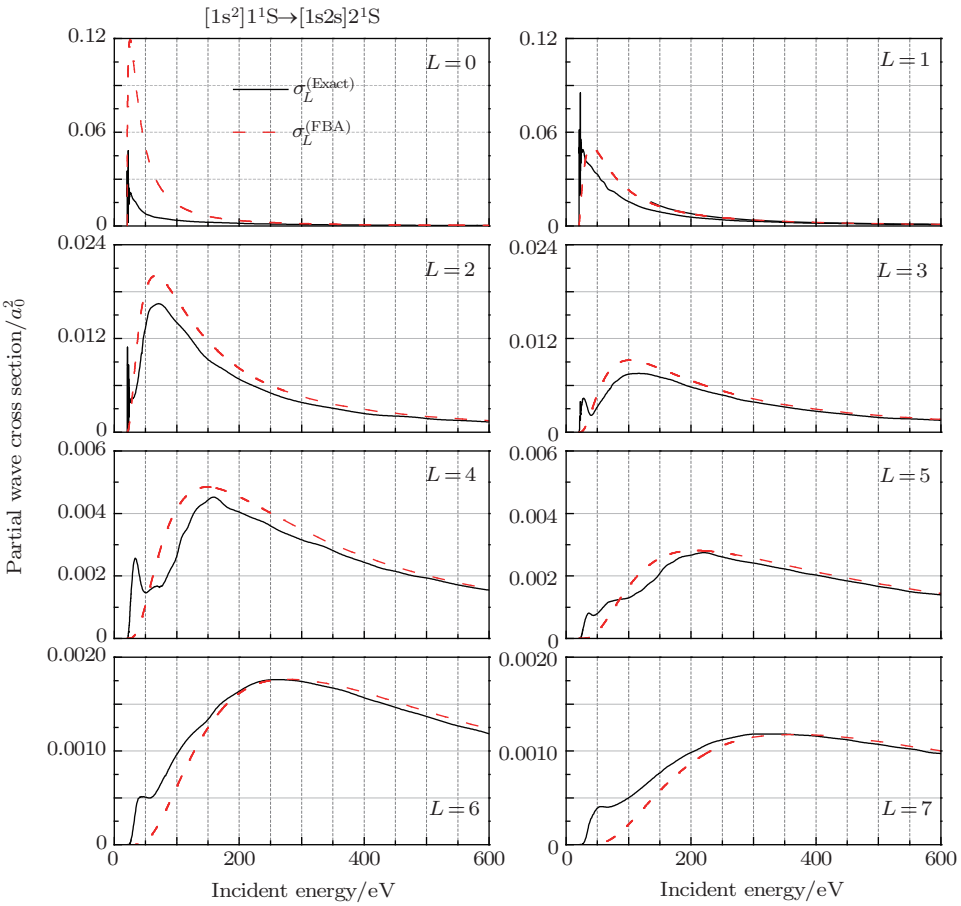


Fig. 1. (color online) The comparisons between the PWCS's ($L = 0$–7) for $[1s^2]1^1S \rightarrow [1s2s]2^1S$ transition calculated according to the formula (4) (solid line labeled as "Exact") and the formula (11) (dashed line labeled as "FBA") respectively.

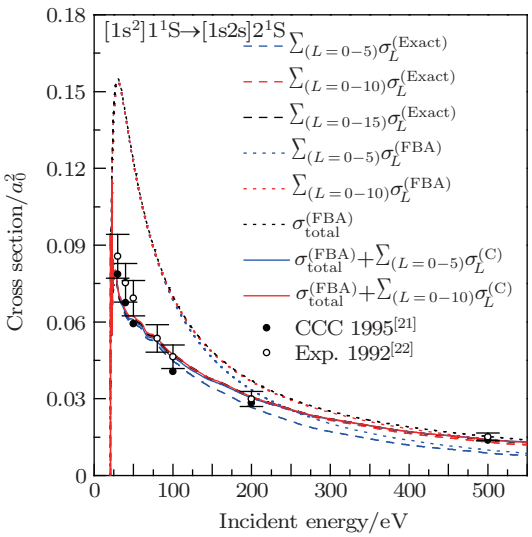


Fig. 2. (color online) The total cross sections for $[1s^2]1^1S \rightarrow [1s2s]2^1S$ transition calculated by the different methods including the partial wave method (labeled as "Exact") and the FBA method (labeled as "FBA").

For more clarity, figure 3 shows the ratios of the calculated total cross sections by different methods in Fig. 2 relative to $\sigma_{\text{total}}^{(\text{FBA})}$. It is known that at the low incident energy the partial wave method is valid and at the high incident energy the FBA is applicable. In Fig. 3, near the excitation threshold the red solid ($\sigma_{\text{total}}^{(\text{FBA})} + \sum_{L=0-10} \sigma_L^{(\text{C})}$) line merges with the red dashed line (calculated by partial wave method), and at the high incident energy the red solid line is closest to one among all the lines, where one means being equal to the FBA results. Therefore, in the overall incident energy range, from threshold to high incident energies, the red solid line converges better than the other results obtained by partial wave or FBA method. This demonstrates that the approach, i.e., replacing the several lowest partial wave cross sections of the total cross sections within FBA by the corresponding exact partial wave cross sections, can deal with the electron impact excitation cross sections of atom for monopole transition from low to high incident energies in an efficient and consistent way. Moreover, the resonance structures are guaranteed since the main resonance features are kept in the lowest several exact PWCS's as shown in Fig. 1.

In Fig. 3, the blue dashed line (the summation of the 6 exact PWCS's) agree with the red solid lines in the range of $E_i/\Delta E < 3$, the red dashed line (the summation of the 11 exact PWCS's) agree with the red solid lines until to $E_i/\Delta E \sim 12$. This demonstrates that at the high incident energies ($E_i/\Delta E > 12$) more PWCS's need to be accounted for the total cross sections. The red and blue dotted lines (the summation of the

FBA PWCS's) start from one at the threshold and then become lower than one gradually. This also means that with the increasing incident energies more FBA PWCS's need to be accounted for in the convergent FBA total cross sections.

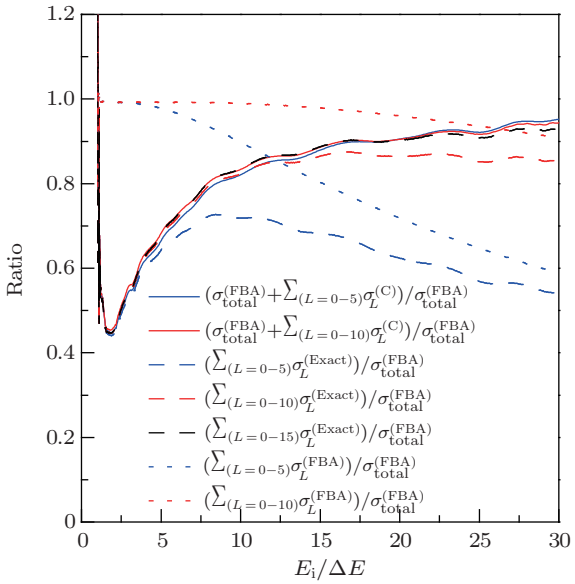


Fig. 3. (color online) The ratios of the calculated total cross section curves by the different methods in Fig. 2 relative to the total cross sections within FBA.

3.2. Dipole transition

Figure 4 shows the comparisons between our calculated eight lowest PWCS's ($L = 0 \sim 7$) for $[1s^2]1^1S \rightarrow [1s2p]2^1P$ transition according to the formula (4) (labeled as "Exact") and the formula (11) (labeled as "FBA") respectively. In Fig. 4, it can be seen that for $L > 0$ the two kinds of PWCS's decrease with the increasing L and the increasing incident energy. The FBA PWCS's decrease faster with the increasing L than the exact PWCS's. On the other hand, the FBA and exact PWCS curves gradually merge together with the increasing L in the overall energy range. Therefore, the main contribution of the difference between $\sigma_{total}^{(Exact)}$ and $\sigma_{total}^{(FBA)}$ should result from the several lowest PWCS's. Comparing with Fig. 1, the PWCS's for dipole transition decrease slower than those for monopole transition, which means the convergent process by using the partial wave method for dipole transition is slower than that for monopole transition, i.e., much more PWCS's need to be accounted for in the convergent total cross sections for dipole transition. In addition, in Fig. 4 the resonance structures mainly display in the exact PWCS's with $L \leq 3$ near the excitation threshold, and no resonance structure appears in the FBA PWCS's.

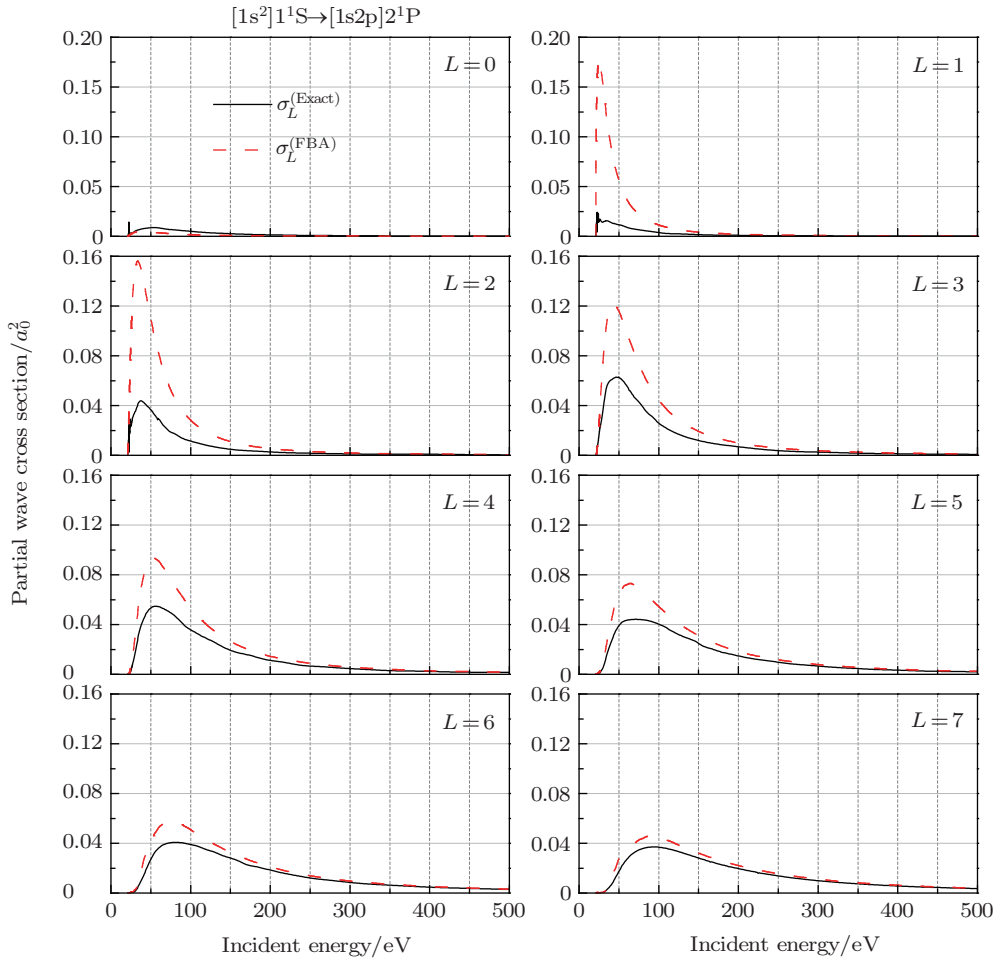


Fig. 4. (color online) The comparisons between the PWCS's for $[1s^2]1^1S \rightarrow [1s2p]2^1P$ transition calculated according to the formula (4) (solid line labeled as "Exact") and the formula (11) (dashed line labeled as "FBA") respectively.

Figure 5 shows the total cross sections for $[1s^2]1^1S \rightarrow [1s2p]2^1P$ transition calculated by partial wave method and FBA method respectively. In Fig. 5, it can be seen that in the whole incident energy range only the red solid line (i.e., $\sigma_{\text{total}}^{(\text{FBA})} + \sum_{L=0-10} \sigma_L^{(\text{C})}$) agrees with the experimental measurement[23] without missing the resonance structures and in a better degree than the CCC theoretical results[21] at the intermediate incident energy around 100 eV. Therefore, the red line can be regarded as our convergent total cross section results. This means the approach of $\sigma_{\text{total}}^{(\text{FBA})}$ plus the summation of limited $\sigma_L^{(\text{C})}$ is applicable to calculate the excitation cross sections for dipole transition. The blue, red, and black dashed lines, i.e., the summations of the lowest 6, 11, and 16 exact PWCS's, agree with the red line only near the threshold and then deviate gradually. For instance, at 200-eV incident energy, the summation of the lowest 16 exact PWCS's is about 0.21, which is only about 66% of the convergent value 0.32. In fact, different from the fast convergence process of monopole transition, for dipole transition the convergence process is slow and it is difficult to obtain the convergent total cross sections by the partial wave method at intermediate and high incident energies. Near the threshold (about 21eV), the summations of the lowest 6 and 11 FBA PWCS's are initially close to and then become smaller than $\sigma_{\text{total}}^{(\text{FBA})}$. At high incident energies (about $E_{\text{i}} > 350$ eV), the summations of PWCS's labeled by "Exact" and "FBA" merge together but are smaller than the FBA total cross sections.

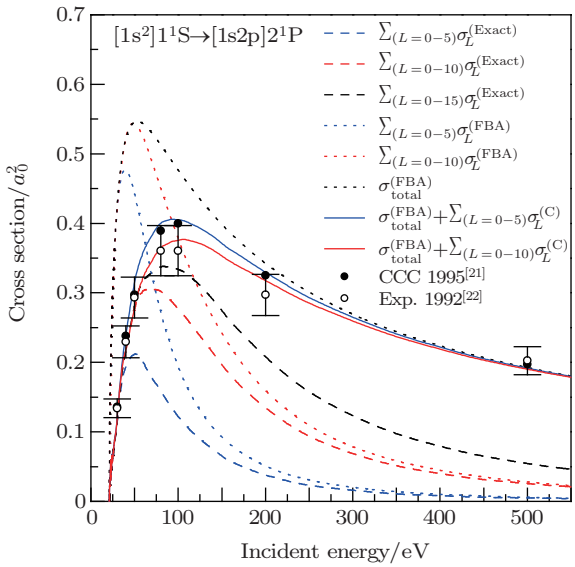


Fig. 5. (color online) The total cross sections for $[1s^2]1^1S \rightarrow [1s2p]2^1P$ transition calculated by the different methods including the partial wave method (labeled as "Exact") and the FBA method (labeled as "FBA").

To see this more clearly, figure 6 shows the ratio curves of the total cross sections calculated by different methods in Fig. 5 relative to $\sigma_{\text{total}}^{(\text{FBA})}$. In Fig. 6, the red solid line is our convergent values. It is obvious that the blue dashed line (the summation of the lowest 6 exact PWCS's) agrees with the red solid line in the range of $E_{\text{i}}/\Delta E < 3$. The red dashed line (the summation of the lowest 11 exact PWCS's) agrees with the red solid line till to $E_{\text{i}}/\Delta E \sim 12$, and for $E_{\text{i}}/\Delta E > 12$ more higher PWCS's need to be accounted for the total cross sections. The ratios of the dotted lines (the summation of the FBA PWCS's) start from one and then deviate gradually. This feature means that with the increasing incident energies more FBA PWCS's need to be accounted for in the FBA total cross sections. On the other hand, with the increasing incident energies the dotted and dashed lines get closer to each other. In the high energy ($E_{\text{i}}/\Delta E > 30$), the value of the red solid line is very close to one. Therefore, for dipole transition, at the intermediate and high incident energies the method of replacing the several lowest partial wave cross sections of the total cross sections within FBA by the corresponding exact partial wave cross sections is more efficient than the partial wave method. Moreover, this method guarantees the resonance structures near the excitation threshold and the satisfaction of FBA at high incident energies.

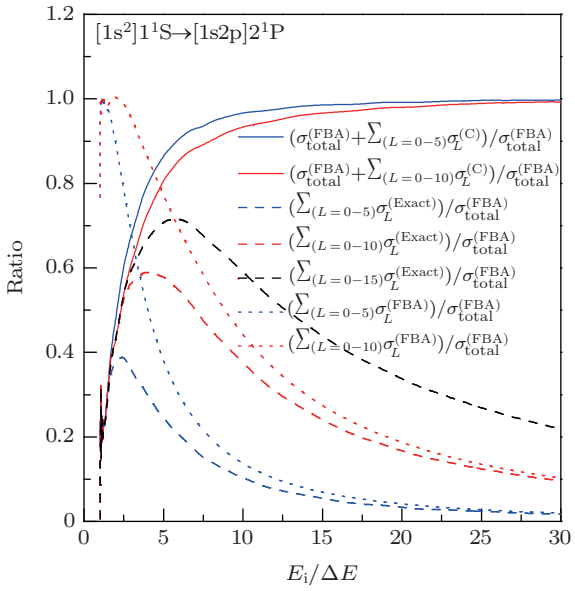


Fig. 6. (color online) The ratios of the calculated total cross section curves by the different methods in Fig. 5 relative to the total cross sections within FBA.

4. Conclusion

Finally we would make the following conclusion. A method to deal with the electron atom collision excitation cross sections from low to high incident energies in a consistent way is presented. This method combines the partial wave method and the FBA method, i.e., replacing the lowest several FBA PWCS's of the FBA total cross sections by the corresponding exact PWCS's. To calculate the FBA PWCS's a new set of codes are developed based on the traditional R-matrix codes. The e–He collision calculations demonstrate the validity and the efficiency of the method for optical-allowed and optical-forbidden transitions. More specifically, our calculated exact and FBA PWCS's of e–He collision decrease with the

increasing angular momentum L and the increasing incident energies. The two kinds of PWCS's merge together with the increasing angular momentum L at intermediate and high incident energies. These features manifest that the difference between the exact and FBA total cross sections mainly originates from the lowest several PWCS's. Thus the convergent total cross sections at low to high incident energy can be obtained by replacing the several lowest partial wave cross sections of the total cross sections within FBA by the corresponding exact partial wave cross sections. Moreover, using this method the resonance structures of the total cross sections near the threshold are guaranteed since the resonances mainly present in the several lowest exact PWCS's near the threshold. Although the CCC method is valid at all incident energies, it concentrates on a single energy at a time and is very time-consuming to exhibit the resonance structures. The illustrated method in this work, inherited from the R-matrix method, has the ability to generate accurate results on a fine energy mesh after the single time consuming step of solving the problem within the 'inner' region and is more timesaving and efficient.

References

[1] Christophorou L G 1971 *Atomic and Molecular Radiation Physics* (New York: John Wiley and Sons Ltd) p. 9
[2] Lindl J D, Amendt P, Berger R L, *et al.* 2004 *Phys. Plasmas* **11** 339
[3] Dalgarno A 1979 *Adv. At. Mol. Phys.* **15** 37
[4] Kallman T R and Palmeri P 2007 *Rev. Mod. Phys.* **79** 79
[5] Beiersdorfer P 2003 *Ann. Rev. Astron. Astrophys.* **41** 343
[6] Smits D P 1996 *Mon. Not. R. Astron. Soc.* **278** 683
[7] Benjamin R A, Skillman E D and Smits D P 1999 *Ap. J.* **514** 307
[8] Kingdon Kunze H J and Johnston III W D 1971 *Phys. Rev. A* **3** 1384
[9] Bray I, Burgess A, Fursa D V and Tully J A 2000 *Astron. Astrophys. Suppl. Ser.* **146** 481
[10] Kingdon J and Ferland G J 1995 *Ap. J.* **442** 714
[11] Bederson B and Kieffer L J 1971 *Rev. Mod. Phys.* **43** 601
[12] Heddle D W O and Gallagher J W 1989 *Rev. Mod. Phys.* **61** 221
[13] Lin C C and Anderson L W 1992 *Adv. At. Mol. Phys.* **29** 1
[14] Nakazaki S 1993 *Adv. At. Mol. Phys.* **30** 1
[15] Berrington K A, Burke P G and Sinfailam A L 1975 *J. Phys. B: At. Mol. Opt. Phys.* **8** 1459
[16] Berrington K A, Burke P G, Freitas L C G and Kingston A E 1985 *J. Phys. B: At. Mol. Opt. Phys.* **18** 4135
[17] Berrington K A and Kingston A E 1987 *J. Phys. B: At. Mol. Opt. Phys.* **20** 6631
[18] Sawey P M J, Berrington K A, Burke P G and Kingston A E 1990 *J. Phys. B: At. Mol. Opt. Phys.* **23** 4321
[19] Sawey P M J and Berrington K A 1993 *At. Data Nucl. Data Tables* **55** 81
[20] Zeng D L, Gao X, Han X Y and Li J M 2015 *Phys. Rev. A* **91** 022707
[21] Fursa D V and Bray I 1995 *Phys. Rev. A* **52** 1279
[22] Fursa D V and Bray I 1997 *J. Phys. B: At. Mol. Opt. Phys.* **30** 757
[23] de heer F J, Hoekstra R, Kingston A E and Summers H P 1992 *Nucl. Fusion Suppl.* **3** 19
[24] Burke P G, Hibbert A and Robb W D 1971 *J. Phys. B: At. Mol. Opt. Phys.* **4** 153
[25] Berrington K A, Burke P G, Chang J J, Chivers A T, Robb W D and Taylor K T 1974 *Comput. Phys. Commun.* **8** 149
[26] Berrington K A, Burke P G, Dourneuf M L, Robb W D, Taylor K T and Voky L 1984 *Comput. Phys. Commun.* **35** C-475
[27] Berrington K A, Burke P G, Butler K, Seaton M J, Storey P J, Taylor K T and Yan Y 1987 *J. Phys. B: At. Mol. Opt. Phys.* **20** 6379
[28] Berrington K A and Kingston A E 1987 *J. Phys. B: At. Mol. Opt. Phys.* **20** 6631
[29] Fano U and Lee C M 1973 *Phys. Rev. Lett.* **31** 1573
[30] Voky L, Saraph H E, Eissner W, Liu Z W and Kelly H P 1992 *Phys. Rev. A* **46** 3945
[31] Berrington K A, Eissner W B and Norrington P H 1995 *Comput. Phys. Commun.* **92** 290
[32] Han X Y and Li J M 2006 *Phys. Rev. A* **74** 062711
[33] Han X Y, Li Y M, Zhang H, Yan J, Li J M and Voky L 2008 *Phys. Rev. A* **78** 052702
[34] Messiah A, 1973 *Quantum Mechanics* (Amsterdam: North-Holland) pp. 312–318
[35] Burke V M and Noble C J 1995 *Comput. Phys. Commun.* **85** 471
[36] Bethe H 1930 *Ann. Phys.* **5** 325
[37] Bethe H 1932 *Z. Phys.* **76** 293
[38] Inokuti M 1971 *Rev. Mod. Phys.* **43** 297